International Journal of Heat and Mass Transfer 52 (2009) 70–78

Contents lists available at ScienceDirect

International Journal of Heat and Mass Transfer

journal homepage: www.elsevier.com/locate/ijhmt

Finite element simulation of natural convection flow in a trapezoidal enclosure filled with porous medium due to uniform and non-uniform heating

Tanmay Basak [a], S. Roy [b], Amit Singh [b], I. Pop [c,*]

[a] Department of Chemical Engineering, Indian Institute of Technology Madras, Chennai 600036, India
[b] Department of Mathematics, Indian Institute of Technology Madras, Chennai 600036, India
[c] Faculty of Mathematics, University of Cluj, CP 253, Cluj, Romania

ARTICLE INFO

Article history:
Received 17 March 2008
Available online 4 August 2008

Keywords:
Penalty finite element method
Natural convection
Porous medium
Trapezoidal cavity
Uniform and non-uniform heating

ABSTRACT

The phenomena of natural convection in a trapezoidal enclosure filled with porous matrix has been studied numerically. A penalty finite element analysis with bi-quadratic elements is performed to investigate the influence of uniform and non-uniform heating of bottom wall while two vertical walls are maintained at constant cold temperature and the top wall is well insulated. Parametric study for the wide range of Rayleigh number Ra ($10^3 \leqslant Ra \leqslant 10^5$), Prandtl number Pr ($0.015 \leqslant Pr \leqslant 1000$) and Darcy number ($10^{-3} \leqslant Da \leqslant 10^{-5}$) shows consistent performance of the present numerical approach to obtain the solutions in terms of stream function and isotherm contours. For parameters studied in the above range, a symmetry is observed for temperature and flow simulations. Non-uniform heating of the bottom wall produces greater heat transfer rate at the center of the bottom wall than uniform heating case for all Rayleigh and Darcy numbers but average Nusselt number shows overall lower heat transfer rate for non-uniform heating case. It is observed that the conduction is dominant irrespective of Ra for $Da = 10^{-5}$. As Rayleigh number increases, there is a change from conduction dominant region to convection dominant region for $Da = 10^{-3}$. The correlations between average Nusselt number and three parameters (Rayleigh number (Ra), Prandtl number (Pr) and Darcy number (Da)) are also obtained.

1. Introduction

Natural convection in a closed cavity is important in many engineering applications. Most of the commonly used enclosures in industries are cylindrical, triangular, rectangular and trapezoidal etc. Buoyancy driven phenomena in enclosures filled with porous medium are actively under investigation for several years. Non-Darcy effects on natural convection in porous media have received significant attention in recent years. This is due to the large number of technical applications such as thermal insulating system, separation process in chemical industries, dispersion of chemical contaminants through water saturated soil, solidification of casting, migration of moisture in grain storage system, crude oil production etc. As a result, this subject has been studied in diverse areas of meteorology, geophysics, energy storage, fire control, greenhouses, solar distillers, growth of crystals in liquids etc. [1–9].

Earlier studies on the convection patterns in various enclosures filled with a porous media are reported in literature by Bejan and Poulikakos [10], Nield and Bejan [11], Ingham and Pop [12] and Poulikakos et al. [13]. The buoyancy driven convection in a differentially heated porous cavity has been analyzed by Walker and Homsy [14] with a number of different techniques. Tong and Subramanian [15] and Lauriat and Prasad [16] further considered Brinkman-extended Darcy model to examine the buoyancy effects on free convection in vertical cavity. This model has been introduced by Brinkman [17] in order to account for the transition from Darcy flow to highly viscous flow, in the limit of high permeability. However, this model does not provide adequate description for the transition from the porous medium flow to pure fluid flow for porous medium with high permeability. A model that bridges the gap between the Darcy and Navier Stokes equations is the Darcy–Forchheimer model [18]. In addition, Darcy–Forchheimer model also describes the effect of inertia and viscous forces in the porous media and was used by Poulikakos and Bejan [19], Lauriat and Prasad [20] to investigate the natural convection in a vertical enclosure filled with a porous medium.

A recent investigation includes the effect of viscous dissipation for Darcy model as studied by Saeid and Pop [21]. Their study shows that the viscous dissipation effect reduces the heat transfer rate and the average Nusselt number in porous cavity decreases with the increase of the viscous dissipation parameter. In another recent investigation Basak et al. [22] studied numerically the natural convection flows in a square cavity filled with a porous matrix for various boundary conditions and wide range of parameters. They found that non-uniform heating of the bottom wall produces

* Corresponding author.
E-mail address: pop.ioan@yahoo.co.uk (I. Pop).

0017-9310/$ - see front matter © 2008 Elsevier Ltd. All rights reserved.
doi:10.1016/j.ijheatmasstransfer.2008.03.032

Nomenclature

Da	Darcy number
g	acceleration due to gravity, m s^{-2}
k	thermal conductivity, W m^{-1} K^{-1}
H	height of the trapezoidal cavity, m
Nu	local Nusselt number
p	pressure, Pa
P	dimensionless pressure
Pr	Prandtl number
R	Residual of weak form
Ra	Rayleigh number
T	temperature, K
T_h	temperature of hot bottom wall, K
T_c	temperature of cold inclined wall, K
u	*x* component of velocity
U	*x* component of dimensionless velocity
v	*y* component of velocity
V	*y* component of dimensionless velocity
X	dimensionless distance along *x* coordinate
Y	dimensionless distance along *y* coordinate

Greek symbols

α	thermal diffusivity, m^2 s^{-1}
β	volume expansion coefficient, K^{-1}
γ	penalty parameter
θ	dimensionless temperature
ν	kinematic viscosity, m^2 s^{-1}
ρ	density, kg m^{-3}
φ	inclination of side wall with vertical line
Φ	basis functions
ψ	stream function
ξ	horizontal coordinate in a unit square
η	vertical coordinate in a unit square

Subscripts

b	bottom wall
l	left wall
r	right wall
s	side wall

greater heat transfer rate at the center of the bottom wall than uniform heating case for all Rayleigh numbers (*Ra*), but average Nusselt numbers (*Nu*) show overall lower heat transfer rates for non-uniform heating case.

An earlier study on natural convection on trapezoidal porous enclosure has been carried out by Baytas and Pop [23]. They solved the problem by finite-difference method with boundary conditions as top enclosure being cooled, bottom cylindrical surfaces being heated and the remaining two non-parallel plane sidewalls of enclosure being adiabatic. Although their study deals with heat transfer studies on various application in trapezoidal porous spaces, a comprehensive analysis on heat transfer and flow circulations is yet to appear in literature.

The aim of the present paper is to provide a complete understanding about the problem, solution procedure and detailed analysis of the temperature and the flow fields on heat transfer evaluation for various materials. The geometry of trapezoidal enclosure with boundary conditions is shown in Fig. 1. The Darcy–Forchheimer model without the Forchheimer's inertia term has been adopted. In the current study, we have used Galerkin finite element method with penalty parameter to solve the nonlinear coupled partial differential equations governing flow and temperature fields for both uniform and sinusoidally varying temperature distribution prescribed at the walls. Non-orthogonal grid generation has been done with iso-parametric mapping [24,25]. The complete explanation about grid generation using iso-parametric mapping is given in Appendix A. Numerical results are obtained to display the circulations and temperature distributions within the trapezoidal enclosure and the heat transfer rate for the bottom and side walls in terms of local and average Nusselt numbers.

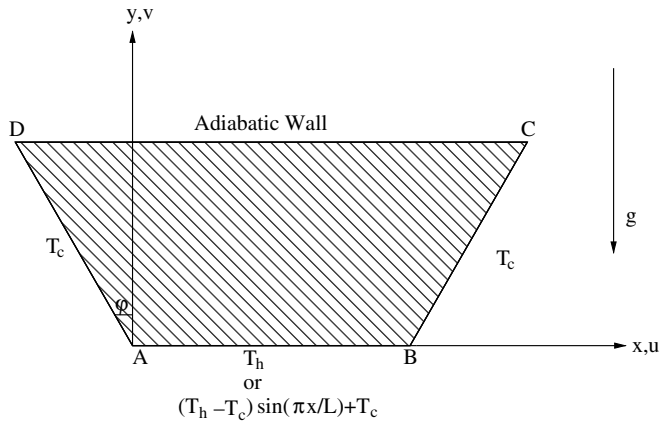

Fig. 1. Schematic diagram of the physical system.

2. Governing equations

Consider a fluid saturated porous medium enclosed in a trapezoidal cavity. It is assumed that the bottom wall is heated either uniformly or non-uniformly while the top wall is well insulated. The vertical walls are assumed to be cooled to a constant temperature. The physical domain is shown in Fig. 1. Thermophysical properties of the fluid in the flow field are assumed to be constant except the density variations causing a body force term in the momentum equation. The Boussinesq approximation is invoked for the fluid properties assuming the variation of density with temperature and to couple in this way the temperature field to the flow field. Further, it is assumed that the temperature of the fluid phase is equal to the temperature of the solid phase in the porous region and local thermal equilibrium (LTE) is applicable in the present investigation [11]. Also, a velocity square term could be incorporated in the momentum equations to model the inertia effect which is more important for non-Darcy effect on the convective boundary layer flow over the surface of a body embedded in a high porosity media. However, this term has been neglected in the present study as the current study involves the natural convection flow in a cavity filled with a porous medium. Under these assumptions and following the earlier works ([18,26]) with the Forchheimer's inertia term neglected, the dimensionless form of governing equations for steady two-dimensional natural convection flow in the porous cavity using conservation of mass, momentum and energy can be written as:

$$\frac{\partial U}{\partial X}+\frac{\partial V}{\partial Y}=0, \tag{1}$$

$$U\frac{\partial U}{\partial X}+V\frac{\partial U}{\partial Y}=-\frac{\partial P}{\partial X}+Pr\left(\frac{\partial^2 U}{\partial X^2}+\frac{\partial^2 U}{\partial Y^2}\right)-\frac{Pr}{Da}U, \tag{2}$$

$$U\frac{\partial V}{\partial X}+V\frac{\partial V}{\partial Y}=-\frac{\partial P}{\partial Y}+Pr\left(\frac{\partial^2 V}{\partial X^2}+\frac{\partial^2 V}{\partial Y^2}\right)-\frac{Pr}{Da}V+RaPr\theta, \tag{3}$$

$$U\frac{\partial \theta}{\partial X}+V\frac{\partial \theta}{\partial Y}=\frac{\partial^2 \theta}{\partial X^2}+\frac{\partial^2 \theta}{\partial Y^2}. \tag{4}$$

where

$$X=\frac{x}{L},\quad Y=\frac{y}{L},\quad U=\frac{uL}{\alpha},\quad V=\frac{vL}{\alpha},\quad \theta=\frac{T-T_c}{T_h-T_c}$$
$$P=\frac{pL^2}{\rho\alpha^2},\quad Pr=\frac{v}{\alpha},\quad Da=\frac{K}{L^2},\quad Ra=\frac{g\beta(T_h-T_c)L^3}{v\alpha}. \tag{5}$$

Here X and Y are dimensionless coordinates varying along horizontal and vertical directions, respectively; U and V are dimensionless velocity components in the X and Y directions, respectively; θ is the dimensionless temperature; P is the dimensionless pressure; Da, Ra and Pr are Darcy, Rayleigh and Prandtl numbers, respectively.

The dimensionless form of boundary conditions are:

$$\begin{aligned}
&U=0,\quad V=0,\quad \theta=1,\text{or}\theta=\sin(\pi X),\quad \forall Y=0,\quad 0\leqslant X\leqslant 1\\
&U=0,\quad V=0,\quad \theta=0,\quad \forall X\cos(\varphi)+Y\sin(\varphi)=0,\quad 0\leqslant Y\leqslant 1\\
&U=0,\quad V=0,\quad \theta=0,\quad \forall X\cos(\varphi)-Y\sin(\varphi)=\cos(\varphi),\quad 0\leqslant Y\leqslant 1\\
&U=0,\quad V=0,\quad \frac{\partial\theta}{\partial Y}=0,\quad \forall Y=1,\quad -\tan(\varphi)\leqslant X\leqslant 1+\tan(\varphi).
\end{aligned} \tag{6}$$

3. Solution procedure

The momentum and energy balance equations [Eqs. (2)–(4)] are solved using the Galerkin finite element method. The continuity equation [Eq. (1)] has been used as a constraint due to mass conservation and this constraint may be used to obtain the pressure distribution. In order to solve Eqs. (2) and (3), we use the penalty finite element method where the pressure P is eliminated by a penalty parameter γ and the incompressibility criteria given by Eq. (1) results in

$$P=-\gamma\left(\frac{\partial U}{\partial X}+\frac{\partial V}{\partial Y}\right). \tag{7}$$

The continuity equation [Eq. (1)] is automatically satisfied for large values of γ. Typical values of γ that yield consistent solutions are 10^7. Using Eq. (7), the momentum balance equations [Eqs. (2) and (3)] reduce to

$$U\frac{\partial U}{\partial X}+V\frac{\partial U}{\partial Y}=\gamma\frac{\partial}{\partial X}\left(\frac{\partial U}{\partial X}+\frac{\partial V}{\partial Y}\right)+Pr\left(\frac{\partial^2 U}{\partial X^2}+\frac{\partial^2 U}{\partial Y^2}\right)-\frac{Pr}{Da}U, \tag{8}$$

and

$$U\frac{\partial V}{\partial X}+V\frac{\partial V}{\partial Y}=\gamma\frac{\partial}{\partial Y}\left(\frac{\partial U}{\partial X}+\frac{\partial V}{\partial Y}\right)+Pr\left(\frac{\partial^2 V}{\partial X^2}+\frac{\partial^2 V}{\partial Y^2}\right)-\frac{Pr}{Da}V+RaPr\theta. \tag{9}$$

The system of equations [Eqs. (4), (8) and (9)] with boundary conditions [Eq. (6)] are solved by using Galerkin finite element method [24]. Since the solution procedure is explained in an earlier work [22], the detailed description is not included in this paper. The numerical solutions are obtained in terms of the velocity components (U, V) and stream function (ψ) is evaluated using the relationship between the stream function (ψ) and the velocity components [27], where the stream function (ψ) is defined in the usual way as $U=\frac{\partial\psi}{\partial Y}$ and $V=-\frac{\partial\psi}{\partial X}$. It may be noted that, the positive sign of ψ denotes anti-clockwise circulation and the clockwise circulation is represented by the negative sign of ψ. The no-slip condition is valid at all boundaries as there is no cross flow, hence $\psi=0$ is used for the boundaries. For steady flows, stream lines are equivalent to the paths followed by the individual particles in the fluid.

The heat transfer coefficient in terms of the local Nusselt number (Nu) is defined by

$$Nu=-\frac{\partial\theta}{\partial n}, \tag{10}$$

where n denotes the normal direction on a plane. The local Nusselt numbers at bottom wall (Nu_b), left wall (Nu_l) and right wall (Nu_r) are defined as

$$Nu_b=-\sum_{i=1}^{9}\theta_i\frac{\partial\Phi_i}{\partial Y} \tag{11}$$

$$Nu_l=-\sum_{i=1}^{9}\theta_i\left(\cos\varphi\frac{\partial\Phi_i}{\partial X}+\sin\varphi\frac{\partial\Phi_i}{\partial Y}\right), \tag{12}$$

and

$$Nu_r=-\sum_{i=1}^{9}\theta_i\left(\cos\varphi\frac{\partial\Phi_i}{\partial X}-\sin\varphi\frac{\partial\Phi_i}{\partial Y}\right). \tag{13}$$

The average Nusselt numbers at the bottom, left and right walls are

$$\overline{Nu_b}=\frac{\int_0^1 Nu_b dX}{X|_0^1}=\int_0^1 Nu_b dX, \tag{14}$$

$$\overline{Nu_l}=\cos\varphi\int_0^{\frac{1}{\cos\varphi}} Nu_l ds_1, \tag{15}$$

and

$$\overline{Nu_r}=\cos\varphi\int_0^{\frac{1}{\cos\varphi}} Nu_r ds_2, \tag{16}$$

where ds_1, ds_2 is the small elemental length along the left and right walls, respectively.

4. Results and discussion

4.1. Numerical tests

The trapezoidal enclosure with $\varphi=30^\circ$ (Fig. 1) has been considered for simulation studies. The computational domain consists of 20×20 bi-quadratic elements which correspond to 41×41 grid points in ξ–η domain as seen in Fig. 2. The bi-quadratic elements with lesser number of nodes smoothly capture the non-linear variations of the field variables which are in contrast with finite-difference solution available in the literature [23]. In order to assess the accuracy of the numerical procedure, we have benchmarked our algorithm based on the grid size for the fluid filled trapezoidal cavity [28]. Also, the result is in well agreement with an earlier work [20] for porous square enclosure with heated side wall.

Numerical solutions are obtained for various values of $Ra = 10^3$–10^5, $Pr = 0.015$–1000 and $Da = 10^{-5}$–10^{-3} with uniform and non-uniform heating of the bottom wall whereas two vertical walls are cooled and the top wall is well insulated. The jump discontinuity in Dirichlet type of wall boundary conditions at the corner point (see Fig. 1) corresponds to computational singularity. To ensure the convergence of the numerical solution to the exact solution, the grid sizes have been optimized and the results presented here are independent of grid sizes. In particular, the singularity at the corner nodes of the bottom wall needs special attention. The grid size dependent effect of the temperature discontinuity at the corner points upon the local (and the overall) Nusselt numbers tend to increase as the mesh spacing at the corner is reduced. One of the ways for handling the problem is assuming the average temperature of the two walls at the corner and keeping the adjacent grid-nodes at the respective wall temperatures. Alternatively, based on earlier work by Ganzarolli and Milanez [29], this procedure is still grid dependent unless a sufficiently refined mesh is

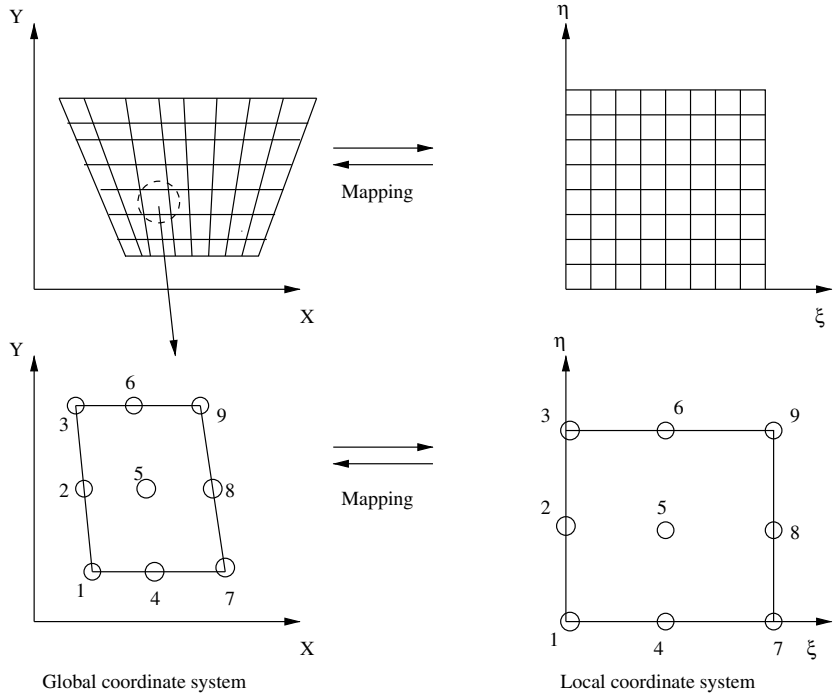

Fig. 2. (a) The mapping of trapezoidal domain to a square domain in ξ–η coordinate system and (b) the mapping of an individual element in ξ–η coordinate system.

implemented. Accordingly, once any corner formed by the intersection of two differently heated boundary walls is assumed at the average temperature of the adjacent walls, the optimal grid size obtained for each configuration corresponds to the mesh spacing over which further grid refinements lead to grid invariant results in both heat transfer rates and flow fields.

In the current investigation, Gaussian quadrature based finite element method provides the smooth solutions at the interior domain including the corner regions as evaluation of residual depends on interior Gauss points and thus the effect of corner nodes is less pronounced in the final solution. The present finite element approach offers special advantage on evaluation of local Nusselt number at the bottom and side walls as the element basis functions are used to evaluate the heat flux.

4.2. Isotherms and streamlines: Uniform heating at bottom wall

Figs. 3–7 illustrate the stream function and isotherm contours for various $Ra = 10^3$–10^5, $Da = 10^{-5}$–10^{-3} and $Pr = 0.015$–1000 when the bottom wall is uniformly heated and the side walls are cooled while the top wall is well insulated. Due to the hot bottom wall, the fluid near to that wall is hotter than the fluid near to cold wall and hence fluid near to hot bottom wall have lower density than that near to the vertical wall. As a result, fluids rise up from middle portion of the bottom wall and flow down along the two vertical walls forming two symmetric rolls with clockwise and anticlockwise rotations inside the cavity. Results indicate that the streamlines and isotherms are strongly dependent on Darcy number as seen in Figs. 3–5.

Fig. 3 displays the temperature and stream function contours for $Da = 10^{-5}$, $Pr = 0.7$ and $Ra = 10^5$. In this case, the flow is seen to be very weak as the maximum value of stream function is found to be 0.032. The temperature contours are smooth and monotonic which illustrate that heat transfer is purely due to conduction. The convection starts playing a dominant role for $Da = 10^{-4}$ with $Ra = 10^5$ and $Pr = 0.7$ (see Fig. 4). A slightly stronger convection pushes the isotherms towards the walls. It is observed that the contours with $\theta \leqslant 0.3$ are pushed towards cold vertical wall whereas $\theta \geqslant 0.4$ contours are continuous curves. It is interesting to observe that the maximum value of stream function is 0.32 as seen from Fig. 4.

As Da increases to 10^{-3}, the strength of the circulation increases (see Fig. 5). The critical Rayleigh number for the conduction dominant mode is found as $Ra = 8 \times 10^3$ for $Da = 10^{-3}$ and $Pr = 0.7$, i.e., conduction is dominant below critical Ra. The value of critical Ra has been obtained from asymptotes of average Nusselt number vs. Rayleigh number plot as discussed later. It is observed that, the flow is strongly dependent on Ra for $Da = 10^{-3}$. For

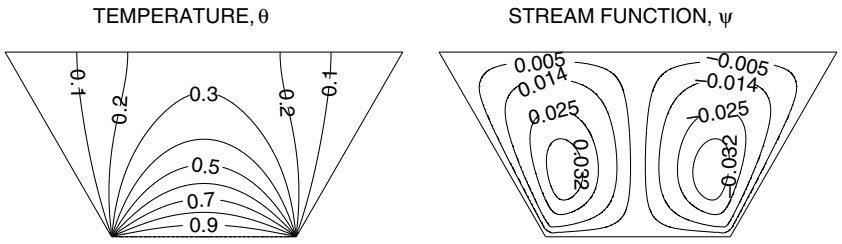

Fig. 3. Contour plots for uniform bottom heating, $\theta(X, 0) = 1$, with $Pr = 0.7$, $Ra = 10^5$ and $Da = 10^{-5}$. Clockwise and anti-clockwise flows are shown via negative and positive signs of stream function, respectively.

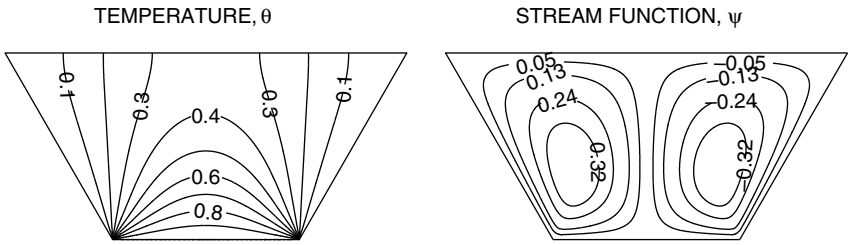

Fig. 4. Contour plots for uniform bottom heating, $\theta(X,0)=1$, with $Pr = 0.7$, $Ra = 10^5$ and $Da = 10^{-4}$. Clockwise and anti-clockwise flows are shown via negative and positive signs of stream function, respectively.

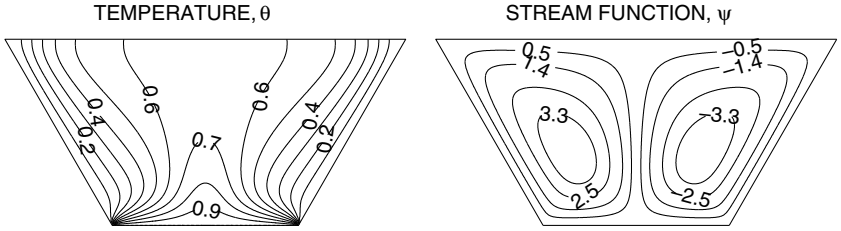

Fig. 5. Contour plots for uniform bottom heating, $\theta(X,0)=1$, with $Pr = 0.7$, $Ra = 10^5$ and $Da = 10^{-3}$. Clockwise and anti-clockwise flows are shown via negative and positive signs of stream function, respectively.

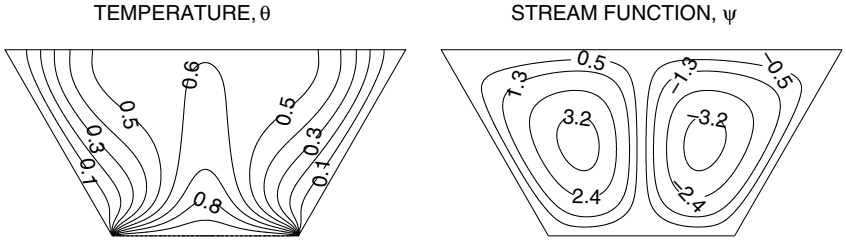

Fig. 6. Contour plots for uniform bottom heating, $\theta(X,0)=1$, with $Pr = 0.015$, $Ra = 10^5$ and $Da = 10^{-3}$. Clockwise and anti-clockwise flows are shown via negative and positive signs of stream function, respectively.

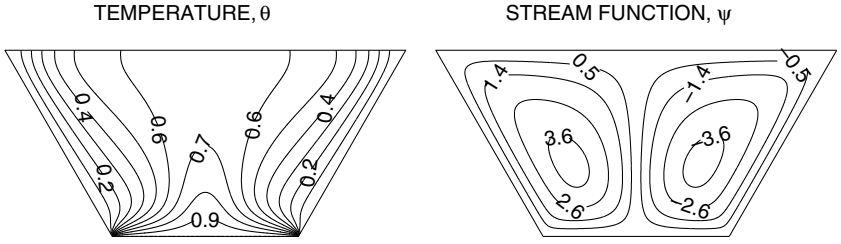

Fig. 7. Contour plots for uniform bottom heating, $\theta(X,0)=1$, with $Pr = 1000$, $Ra = 10^5$ and $Da = 10^{-3}$. Clockwise and anti-clockwise flows are shown via negative and positive signs of stream function, respectively.

$Da = 10^{-3}$ and $Ra = 10^5$, the circulation near the central regimes are stronger and consequently, the temperature contours with $\theta \leqslant 0.6$ start getting shifted towards the side walls and they break into two symmetric contour lines (see Fig. 5). The presence of significant convection is also exhibited in temperature contour lines which start getting deformed and pushed towards the side walls. The intensity of circulation is greater near the center and least near the walls due to no slip conditions. The greater circulation in each half of the box follows a progressive wrapping around the centers of rotation, and a more and more pronounced compression of isotherms towards the boundary surfaces of the enclosures occurs. Consequently, near the central core at the top half of the enclosure, there are small gradients in temperature whereas a large stratification zone of temperature is observed at the vertical symmetric line near the bottom wall. Fig. 6 shows that intensity of stream function and isotherms in a core cavity decreases for $Pr = 0.015$. Due to less circulation, the zone of stratification of temperature at the central symmetric line is increased. In contrast, due to greater circulation at $Pr = 1000$ (Fig. 7), the zone of stratification of temperature at the central symmetric lines is reduced. Similar to previous cases, the isotherms are pushed along the vertical walls due to enhanced circulations in the central regime at higher Ra for $Da = 10^{-3}$.

4.3. Isotherms and streamlines: Non-uniform heating at bottom wall

Streamlines and isotherms are displayed in Figs. 8–10 for $Ra = 10^5$, $Da = 10^{-3}$ corresponding to $Pr = 0.7$, 0.015 and 1000, respectively, when the bottom wall is non-uniformly heated via

sinusoidal function. As seen in Figs. 3–7, uniform heating of bottom wall causes a finite discontinuity in Dirichlet type of boundary conditions for the temperature distribution at both edges of the bottom wall. In contrast, the non-uniform heating removes the singularity at the edges of bottom wall and provides a smooth temperature distribution in the entire enclosure. For $Da = 10^{-5}$ and $Pr = 0.7$, the isotherms (figure not shown) are similar to that with uniform heating case as seen in Fig. 3. The heat transfer is primarily due to the conduction and similar phenomenon was observed with uniform heating case. It is interesting to note that, the temperature at the bottom wall is non-uniform and maxima in temperature occurs at the center. Therefore the greater heat transfer rate will occur at the center and the detailed analysis will be illustrated in the following section.

At $Da = 10^{-3}$, $Pr = 0.7$ and $Ra = 10^5$ the circulation pattern is qualitatively similar to the uniform heating case with the identical situation (see Fig. 8). Due to non-uniform bottom heating, the heating rate is generally lower and that induces less buoyancy effect. The critical value of Rayleigh number for conduction dominant heat transfer corresponding to $Da = 10^{-3}$ and $Pr = 0.7$ is upto $Ra = 5 \times 10^3$ which is less than for uniform heating case which corresponds to critical $Ra = 8 \times 10^3$. Further compared to uniform heating case, the magnitude of isotherms are less near the central and top portion of the enclosure for non-uniform heating case. The greater values of isotherms are highly dense near the center of the bottom wall which may indicate a greater local heating rate compared to uniform heating case (see Figs. 8–10).

Figs. 9 and 10 show stream function and temperature contours for $Pr = 0.015$ and $Pr = 1000$, respectively with $Ra = 10^5$ and $Da = 10^{-3}$. It is interesting to observe that the maximum value of stream function is 3 for $Pr = 0.7$ whereas that is 2.5 for $Pr = 0.015$ and 3.2 for $Pr = 1000$. Also, it is observed that the temperature contours with $\theta \leqslant 0.3$ are pushed towards the vertical wall for $Pr = 0.015$ (Fig. 9) whereas contours with $\theta \leqslant 0.4$ have been pushed for $Pr = 0.7$ and $Pr = 1000$ (Figs. 8 and 10).

4.4. Heat transfer rates: Local Nusselt numbers

Fig. 11(a) and (b) display the effect of Da (10^{-5}–10^{-3}) and $Pr = 0.7$ on the local Nusselt numbers at the bottom and side walls (Nu_b, Nu_s). For the uniform heating of the bottom wall (Fig. 11(a)), due to the presence of discontinuity in the temperature boundary condition at the edges of bottom wall, the heat transfer rate is very high at these corners and this is common to all Darcy and Prandtl numbers. In addition, the heat transfer rate reduces towards the middle of the bottom wall as the isotherms are well dispersed at the middle. In contrast, for $Da = 10^{-5}$ and $Da = 10^{-4}$ with non-uniformly heated bottom wall, Nu_b increases from zero at both the edges of the bottom wall towards the center where a maximum value is observed. The local maxima of Nu_b for non-uniform heating is due to the fact that higher degree of compression of isotherms occur near the central regime. On the other hand, the temperature contours diverge from the corner points towards the central vertical line for uniform heating case and therefore the local Nusselt number monotonically decreases from the corner point to the center. Further, for $Da = 10^{-3}$, the non-uniform heating produces a sinusoidal type of local heat transfer rate with its minimum value at the edges as well as at the center of the bottom wall. Two maxima in Nu_b is obtained as the isotherms are compressed at $X = 0.3$ and 0.7. This is due to fact that the higher intensity of circulations compresses the isotherms at $X = 0.3$ and $X = 0.7$. It is also noticed that for all regimes of Darcy and Rayleigh numbers, the heat transfer rate at the central regime for the non-uniform heating is larger than that for uniform heating.

Fig. 11(b) illustrates the heat transfer rate at the side wall. At the bottom corner points, Nu_s is large due to discontinuity in temperature for uniform heating case whereas due to dispersed temperature contours or less thermal gradient, the heat transfer rate for non-uniform case is lesser than that for uniform heating case irrespective of Pr and Da. The local Nusselt number (Nu_s) decreases with distance at the side wall for $Da = 10^{-5}$ and $Da = 10^{-4}$ with $Pr = 0.7$ for both uniform and non-uniform heating cases. On the other hand, for $Da = 10^{-3}$, the heat transfer rate initially decreases and later increases with distance. This is due to compressed isotherms towards the side walls away from the corner points at the bottom for $Da = 10^{-3}$. Therefore, the heat transfer rates are enhanced at the regimes away from bottom corner points. It is observed that at higher Rayleigh number, the significant circulation results in dense contours at the top portion of the side walls and these dense isotherms are in contrast with the conduction dominant cases. The degree of compression of isotherms at the top portion is less for non-uniform heating case.

4.5. Overall heat transfer rate and average Nusselt numbers

The overall effects upon the heat transfer rates are displayed in Fig. 12(a–d), where the distributions of the average Nusselt number of bottom and side walls, are plotted vs. the logarithmic Rayleigh number. The average Nusselt numbers were obtained using Eqs. (14)–(16) where the integral is evaluated using Simpson's 1/3 rule. Note that, Figs. 12(a) and (b) (cases a and b) illustrates uniform heating cases and Fig. 12(c) and (d) (cases c and d) illustrate non-uniform heating cases. The average Nusselt numbers for bottom walls remain constant upto $Ra = 8 \times 10^3$ with uniform heating case and upto $Ra = 5 \times 10^3$ with non-uniform heating case when $Pr = 0.7$ and $Da = 10^{-3}$. It may be noted that, the influence of the Rayleigh number on the Nusselt number becomes significant at higher Darcy number. It may also be noted that, average Nusselt number ($\overline{Nu_s}$, $\overline{Nu_b}$) remain invariant of Ra for $Da = 10^{-5}$ irrespective of Pr. This further confirms that the heat transfer is conduction dominant for low Darcy numbers. The average Nusselt numbers at the bottom and side walls were thermally balanced within 1% error. The values of average Nusselt number are more in the case of uniform heating compared to non-uniform heating as seen in the Fig. 12(a–d). The following relationship has been obtained for

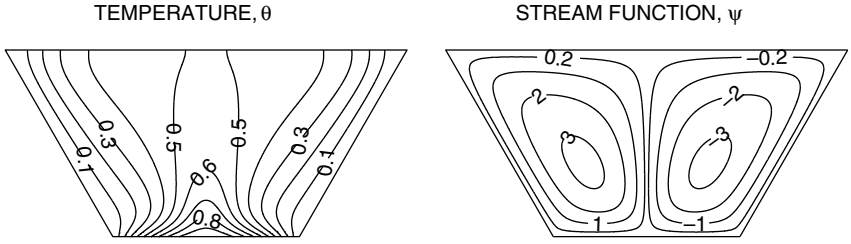

Fig. 8. Contour plots for non-uniform bottom heating, $\theta(X, 0) = sin(\pi X)$, with $Pr = 0.7$, $Ra = 10^5$ and $Da = 10^{-3}$. Clockwise and anti-clockwise flows are shown via negative and positive signs of stream function, respectively.

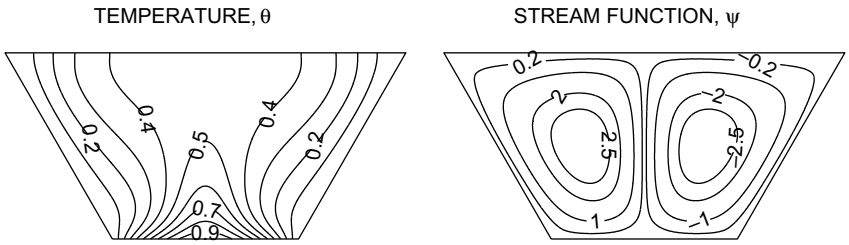

Fig. 9. Contour plots for non-uniform bottom heating, $\theta(X,0) = sin(\pi X)$, with $Pr = 0.015$, $Ra = 10^5$ and $Da = 10^{-3}$. Clockwise and anti-clockwise flows are shown via negative and positive signs of stream function, respectively.

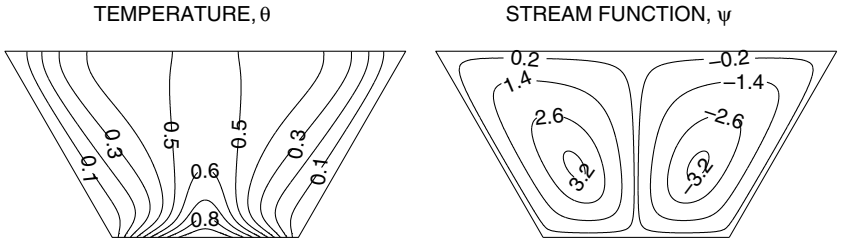

Fig. 10. Contour plots for non-uniform bottom heating, $\theta(X,0) = sin(\pi X)$, with $Pr = 1000$, $Ra = 10^5$ and $Da = 10^{-3}$. Clockwise and anti-clockwise flows are shown via negative and positive signs of stream function, respectively.

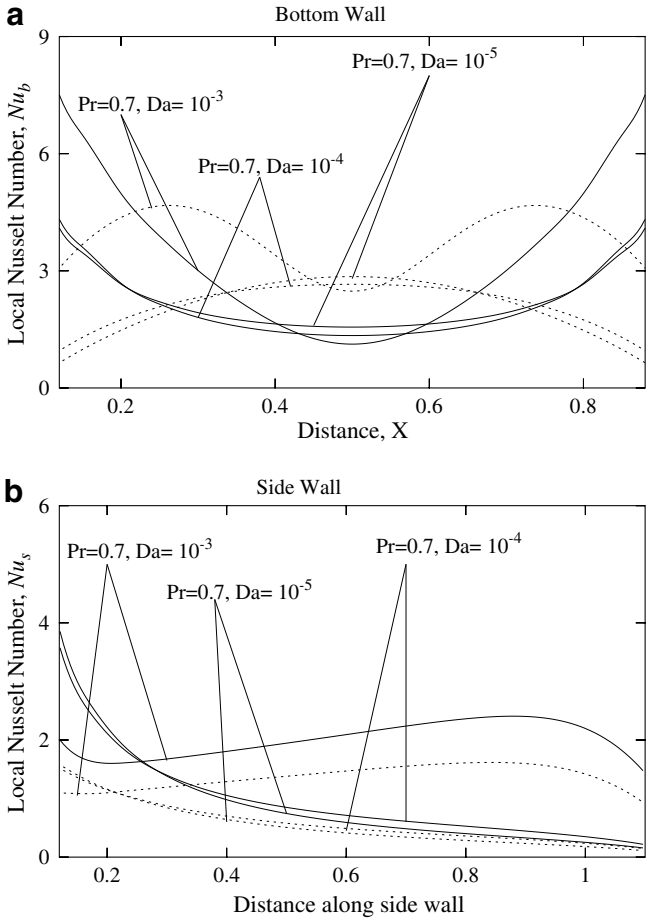

Fig. 11. Variation of local Nusselt number with distance (a) at the bottom wall (b) at the side wall for uniform heating (——) and non-uniform heating (- - -).

uniform and non-uniform heating of bottom wall between average Nusselt number and three parameters (Rayleigh number, *Ra*, Prandtl number, *Pr* and Darcy number, *Da*):

Cases a and b: uniform heating

$$\overline{Nu_b} = 2.308\overline{Nu_s} = 4.0770 Pr^{0.0102} Da^{0.0141} Ra^{0.0144}, \quad Ra \geqslant 8 \times 10^3.$$

Cases c and d: non-uniform heating

$$\overline{Nu_b} = 2.308\overline{Nu_s} = 1.6543 Pr^{0.0194} Da^{0.0415} Ra^{0.05}, \quad Ra \geqslant 5 \times 10^3.$$

5. Conclusion

In the current investigation, the influence of uniform and non-uniform heating of the bottom wall and heat transfer characteristics due to natural convection within a trapezoidal enclosure filled with porous medium has been studied in detail. The penalty finite element method helps to obtain smooth solutions in terms of stream function and isotherm contours for uniform and non-uniform heating of the bottom wall with wide ranges of *Pr*, *Ra* and *Da*. The heat transfer rate is very high at the edges of the bottom wall and decreases to a minimum value at the center especially at the bottom wall due to uniform heating which contrast the lower heat transfer rate at the edges due to non-uniform heating. We observed that the conduction dominant heat transfer modes for $Ra \leqslant 8 \times 10^3$ during uniform heating of bottom wall whereas the conduction dominant heat transfer is observed for $Ra \leqslant 5 \times 10^3$ for non-uniform heating in presence of high Darcy numbers ($Da = 10^{-3}$).

At the onset of convection dominant mode, the temperature contour lines get compressed towards the side walls and they tend to get deformed towards the upward direction. For $Da = 10^{-3}$, thermal boundary layer is developed near the bottom and side walls and the central regime near the top surface has least temperature gradient for both uniform and non-uniform heating cases. In the case of uniform heating of the bottom wall the heat transfer rate attains minimum at the center of the bottom wall and increases towards the edges. In contrast, for the case of non-uniform heating, with $Da \leqslant 10^{-4}$, the heat transfer increases from the left of the bottom wall and attains maximum at the center and then

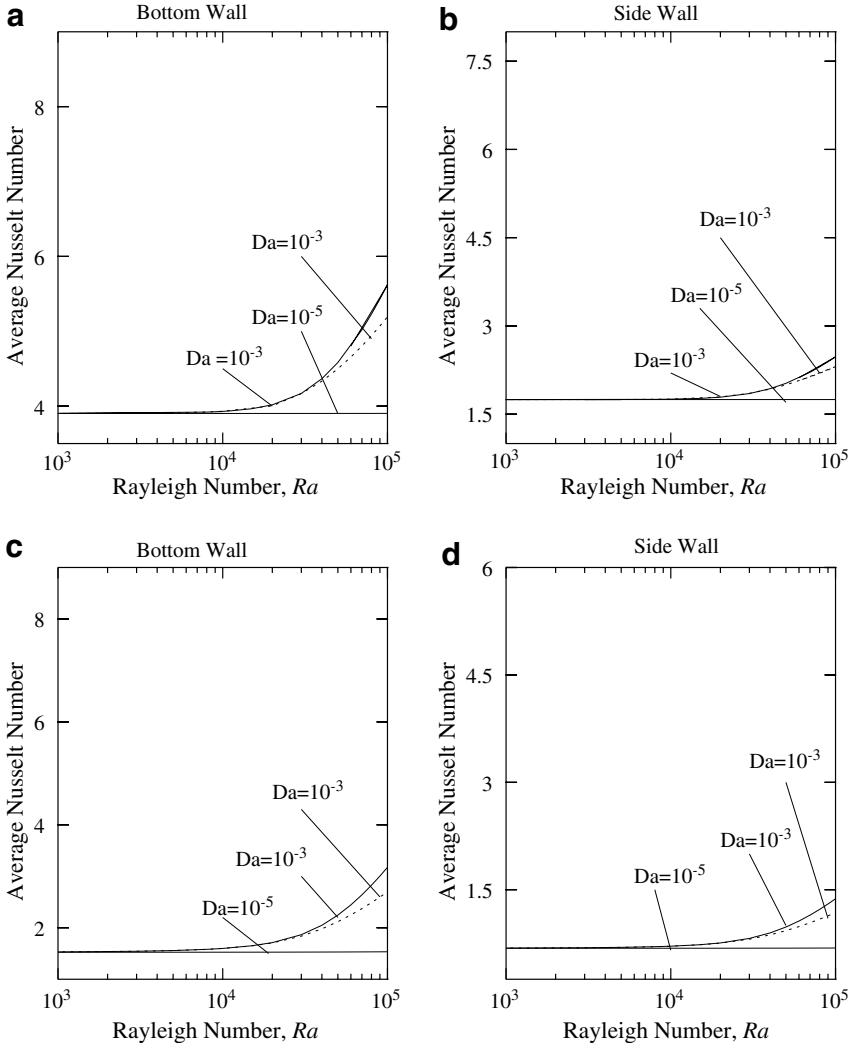

Fig. 12. Variation of average Nusselt number with Rayleigh number for uniform heating [(a) and (b)] and non-uniform heating [(c) and (d)]. The insets show the loglog plot of average Nusselt number vs. Rayleigh number for $Pr = 0.7$ (——) and $Pr = 0.015$ (- - -).

decreases whereas for $Da = 10^{-3}$ a sinusoidal type of heat transfer is obtained. The non-uniform heating exhibits greater heat transfer rates at the center of the bottom wall than the uniform heating case for all parameter regimes. The local Nusselt number at the side wall is found to be decreased with distance for conduction dominant heat transfer whereas Nu_s is found to be increased due to highly dense contour lines near the top portion of the side wall for both uniform and non-uniform heating cases. The average Nusselt numbers illustrate overall lower heat transfer rates for non-uniform heating cases. Finally correlation between average Nusselt number, Rayleigh number, Prandtl number and Darcy number have been obtained for uniform and non-uniform heating cases.

Appendix A

The name "isoparametric" derives from the fact that the same parametric function describing the geometry may be used for interpolating spatial variable within an element. Fig. 2 shows a trapezoidal domain which is mapped to a square domain. The transformation between (x, y) and (ξ, η) coordinates can be defined by $X = \sum_{k=1}^{9} \Phi_k(\xi, \eta) x_k$ and $Y = \sum_{k=1}^{9} \Phi_k(\xi, \eta) y_k$ where (x_k, y_k) are the X, Y coordinates of the k nodal points as seen in Fig. 2a, b and $\Phi_k(\xi, \eta)$ is the basis function. The nine basis functions are:

$$\Phi_1 = (1 - 3\xi + 2\xi^2)(1 - 3\eta + 2\eta^2)$$
$$\Phi_2 = (1 - 3\xi + 2\xi^2)(4\eta - 4\eta^2)$$
$$\Phi_3 = (1 - 3\xi + 2\xi^2)(-\eta + 2\eta^2)$$
$$\Phi_4 = (4\xi - 4\xi^2)(1 - 3\eta + 2\eta^2)$$
$$\Phi_5 = (4\xi - 4\xi^2)(4\eta - 4\eta^2)$$
$$\Phi_6 = (4\xi - 4\xi^2)(-\eta + 2\eta^2)$$
$$\Phi_7 = (-\xi + 2\xi^2)(1 - 3\eta + 2\eta^2)$$
$$\Phi_8 = (-\xi + 2\xi^2)(4\eta - 4\eta^2)$$
$$\Phi_9 = (-\xi + 2\xi^2)(-\eta + 2\eta^2)$$

The above basis functions are used for mapping the trapezoidal domain into square domain and the evaluation of integrals of residuals.

References

[1] O. Laguerre, S.B. Amara, D. Flick, Experimental study of heat transfer by natural convection in a closed cavity: application in a domestic refrigerator, J. Food Eng. 70 (2005) 523–537.
[2] S.M.M. EL-Kabeir, A.M. Rashad, R.S. Reddy Gorla, Unsteady MHD combined convection over a moving vertical sheet in a fluid saturated porous medium with uniform surface heat flux, Math. Comput. Model. 46 (2007) 384–397.
[3] X.Y. You, Estimating the onset of natural convection in a horizontal layer of a fluid with a temperature-dependent viscosity, Chem. Eng. J. 84 (2001) 63–67.

[4] M.M. Al-Hazmy, Analysis of coupled natural convection-conduction effects on the heat transport through hollow building blocks, Energ. Buildings 38 (2006) 515–521.
[5] H. Asan, L. Namli, Laminar natural convection in a pitched roof of triangular cross-section: summer day boundary conditions, Energ. Buildings 33 (2000) 69–73.
[6] D. Jain, G.N. Tiwari, Effect of greenhouse on crop drying under natural and forced convection I: Evaluation of convective mass transfer coefficient, Energ. Convers. Manage. 45 (2004) 765–783.
[7] A. Omri, J. Orfi, S.B. Nasrallah, Natural convection effects in solar stills, Desalination 183 (2005) 173–178.
[8] A. Omri, Numerical investigation on optimization of a solar distiller dimensions, Desalination 206 (2007) 373–379.
[9] A. Nakanoa, H. Ozoea, S.W. Churchill, Numerical computation of natural convection for a low-Prandtl-number fluid in a shallow rectangular region heated from below, Chem. Eng. J. 71 (1998) 175–182.
[10] A. Bejan, D. Poulikakos, The nondarcy regime for vertical boundary layer natural convection in porous medium, Int. J. Heat Mass Tran. 27 (1984) 717–722.
[11] D.A. Nield, A. Bejan, Convection in Porous Media, 2nd ed., Springer, New York, 1999.
[12] D.B. Ingham, I. Pop, Transport Phenomena in Porous Media, Pergamon, 1998.
[13] D. Poulikakos, A. Bejan, B. Selimos, K.R. Blake, High Rayleigh number convection in the fluid overlaying a porous bed, Int. J. Heat Mass Tran. 7 (1986) 109–116.
[14] K.L. Walker, G.M. Homsy, Convection in porous cavity, J. Fluid Mech. 87 (1978) 449–474.
[15] T.W. Tong, E. Subramanian, Boundary layer analysis for natural convection in porous enclosure: use of Brinkman-extended Darcy formulation, Int. J. Heat Mass Tran. 28 (1985) 563–571.
[16] G. Lauriat, V. Prasad, Natural convection in a vertical porous cavity: a numerical study for Brinkman-extended Darcy formulation, Trans. ASME J. Heat Tran. 109 (1987) 295–320.
[17] H.C. Brinkman, On the permeability of media consisting of closely packed porous particles, Appl. Sci. Res. 1 (1947) 81–86.
[18] K. Vafai, C.L. Tien, Boundary and inertia effects on flow and heat transfer in porous media, Int. J. Heat Mass Tran. 24 (1981) 195–203.
[19] D. Poulikakos, A. Bejan, The departure from Darcy flow in natural convection in a vertical porous layer, Int. J. Heat Mass Tran. 28 (1985) 3477–3484.
[20] G. Lauriat, V. Prasad, NonDarcian effects on natural convection in a vertical porous enclosure, Int. J. Heat Mass Tran. 32 (1989) 2135–2148.
[21] N.H. Saeid, I. Pop, Viscous dissipation effects on free convection in a porous cavity, Int. Commun. Heat Mass Tran. 31 (2004) 723–732.
[22] T. Basak, S. Roy, T. Paul, I. Pop, Natural convection in a square cavity filled with a porous medium: effects of various thermal boundary conditions, Int. J. Heat Mass Tran. 49 (2006) 1430–1441.
[23] A.C. Baytas, I. Pop, Natural convection in a trapezoidal enclosure filled with a porous medium, Int. J. Eng. Science 39 (2001) 125–134.
[24] J.N. Reddy, An Introduction to the Finite Element Method, McGraw-Hill, New York, 1993.
[25] T.J. Chung, Computational Fluid Dynamics, Cambridge University Press, London, 2002.
[26] Z.-G. Du, E. Bilgen, Natural convection in vertical cavities with internal heat generating porous medium, Warme-und Stoffubertr 27 (1992) 149–155.
[27] G.K. Batchelor, An Introduction to Fluid Dynamics, Cambridge University Press, 1993.
[28] E. Natarajan, T. Basak, S. Roy, Natural convection flow in a trapezoidal enclosure with uniform and non-uniform heating of bottom wall, Int. J. Heat Mass Tran. 51 (2008) 747–756.
[29] M.M. Ganzarolli, L.F. Milanez, Natural convection in rectangular enclosures heated from below and symmetrically cooled from the sides, Int. J. Heat Mass Tran. 38 (1995) 1063–1073.